

Synthesis and physicochemical properties of CuMn_2O_4 nanoparticles; a potential semiconductor for photoelectric devices

M. Enhessari^{*1}, A. Salehabadi¹, K. Maarofian², S. Khanahmadzadeh²

¹ Department of Chemistry, Naragh Branch, Islamic Azad University, Naragh, Iran

² Department of Chemistry, Mahabad Branch, Islamic Azad University, Mahabad, Iran

Received: 9 March 2016; Accepted: 11 May 2016

ABSTRACT: CuMn_2O_4 nanoparticles, a semiconducting materials with tunable functionalities in solid oxide fuel cell, was successfully synthesized via a sol-gel method using its respective metal cations sources i.e. Cu^{2+} and Mn^{2+} in an appropriate complexing agent. The vibrational frequencies below 1000 cm^{-1} of the obtained materials confirmed the formation of metal-oxygen (M-O:Cu-O, Mn-O) bond in the sample. The structural analysis of the crystalline phase indicates the formation of a series of sharp peaks with particle size about 39 nm. The cubic crystal structure clearly confirmed the formation of CuMn_2O_4 with space group $\text{Fd}\bar{3}\text{m}$ -copper ions occupied the tetrahedral sites according to (111), (220), (311), and (222) Miller index parameters. Heterogeneous morphology of CuMn_2O_4 nanoparticles indicated an agglomerated grain structure. The excitation threshold of photoluminescence (PL) indicated that the CuMn_2O_4 is a medium material in photoluminescence applications. The band gap energy (E_g) equal to 1.4 eV calculated from DR spectra, revealed that CuMn_2O_4 can be used as a semiconducting material in photoelectrical devices. Color scale parameters evaluated by colorimetric analysis resulted characteristic values of $L^*=20.18$, $a^*=2.98$ and $b^*=2.94$.

Keywords: CuMn_2O_4 ; Nanoparticles; Optical band gap; Sol-gel; Semiconductor

INTRODUCTION

Spinel, in general, has the formula AB_2O_4 (Atkins *et al.*, 2006). The spinel structure consists of a ccp array of O^{2-} ions in which the A cations occupy one-eighth of the tetrahedral holes and the B cations occupy half of the octahedral holes (Ishihara 2009). The spinel CuMn_2O_4 as a process efficient the fuel cell with economic and environmental advantages as compared with layered compounds such as CuCo_2O_4 and LiNiO_2 (Kalyani and Kalaiselvi 2005, Sun *et al.*, 2013). The distribution of

the atoms in the structure of CuMn_2O_4 , on the basis of coordination and the local environments for the cations (Fig.1) has been reported by Shoemaker and coworkers (Shoemaker *et al.*, 2009).

Solid-state reaction (Uchimoto *et al.*, 2005), hydrothermal method (Byrappa and Yoshimura 2001), combustion synthesis (Ianos *et al.*, 2012), sol-gel (M. Enhessari *et al.*, 2013, Shaterian *et al.*, 2014) have been reported to synthesize spinels. Among them, the solid-state reaction and combustion synthesis have at-

✉ Corresponding Author - e-mail: enhessari@gmail.com

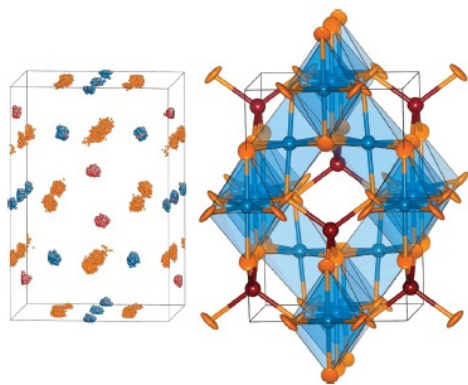


Fig.1. Distribution of the atoms in the crystal structure of CuMn_2O_4

tracted a great attention due to superior performance in production of cathode materials. Mungse *et al.*, (Mungse *et al.*, 2014) have been reported a chemical looping combustion (CLC) as a key technology for oxy-fuel combustion to separate CO_2 from a flue gas, where oxygen is derived from a solid oxygen carrier. Copper-based spinel was proposed as a highly active catalyst for MeOH SR and DME SR (Ishihara 2009). In recent years, fuel cells as a source of clean energy have been achieved a great attention (Ishihara 2009, Oh *et al.*, 2014)

In current study, a wet chemistry synthesis method was performed using stearic acid, copper and manganese acetates as a complexing agent and metal cations sources, respectively. Here, the metal cations diffuse up from aqueous to organic phase above melting point of stearic acid (Enhessari 2013). To complete the pro-

cess, a stepwise thermal program was adjusted from 200 to 600°C. The final products were quenched into the room temperature for further analysis.

MATERIALS AND METHOD

Copper acetate (99.9 % purity, Aldrich) and manganese acetate (99% purity, Aldrich) first dissolved in water, in the molar ratio of $\text{Cu}^{2+}:\text{Mn}^{2+}$, 1:2. The metal ions solution was then added into the melted stearic acid (97 % purity, Merck) container. During this step, the two phases solution abruptly transformed into a viscous gel. The gel was subsequently heated up to the melting point of stearic acid and allowed to evaporate the aqueous phase. A light-pink precursor obtained for further thermolysis. The as prepared precursor was slowly heated up and calcined from 200 to 600°C. The fine nanoparticles obtained from previous calcination were quenched, grinded and mixed up for further investigations.

RESULT AND DISCUSSION

Structural Analysis

Fourier transform infrared spectrometer (FT-IR, Perkin Elmer spectrum RX1) was used to confirm the formation of metal-oxygen (M-O) and metal-metal (M-M) bonds in the coordination structure of the sample.

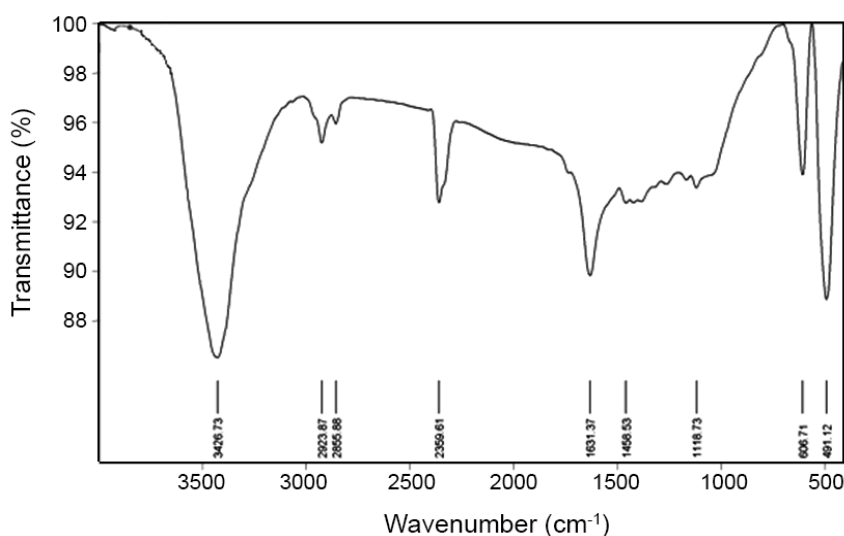


Fig. 2. FT-IR of CuMn_2O_4 calcined at 600°C for 4 h

The sample was mixed with KBr and examined at the wavenumber range from 450 to 4000 cm^{-1} . The vibration frequencies of M-O appear below 1000 cm^{-1} . Two vibrational frequencies at 607 and 491 cm^{-1} confirm the formation of M-O (Cu-O and Mn-O) bonds in the obtained CuMn_2O_4 (Fig. 2). These are the primary evidence of CuMn_2O_4 formation (Mungse *et al.*, 2014).

The crystal structure and the lattice information of the obtained nanoscale CuMn_2O_4 was investigated using Rigaku X-ray diffractometer (XRD, PTS 3003, Cu K_α radiation at 30 kV-20 mA, $2\theta = 10\text{-}90^\circ$). Lattice constants were determined by a least-squares refinement of the d-spacing, which were measured in comparison with an internal standard of pure barium sulfate. The XRD pattern of CuMn_2O_4 nanoparticles (Fig. 3) shows several intense peaks (Indexed in the pattern) which are in well agreement with literature (JCPDS 74-1921). The cubic crystal structure of CuMn_2O_4 can be confirmed by a series of intense peaks. Some of them are located at 2θ equal to 18.94° , 30.85° , 36.00° , and 37.42° , clearly confirm the formation of cubic crystal structure of CuMn_2O_4 . The spinel structure of CuMn_2O_4 with space group $\text{Fd}\bar{3}\text{m}$ -copper ions occupy the tetrahedral sites, can be clearly identified according to (111), (220), (311), and (222) Miller index parameters. The average crystallite size (D) of the nanopowders was calculated from the XRD pattern according to the line width of the plane reflection peak using Scherrer equation (1):

$$D = \frac{k\lambda}{\beta \cos \theta} \quad (1)$$

where θ is the angle, λ is the wavelength (0.15418 nm), β is the width of the XRD peak at half height and k is a shape factor, about 0.9 for spherical shaped nanoparti-

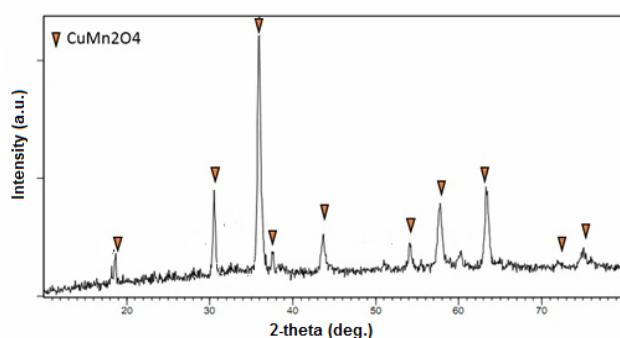


Fig. 3. XRD pattern of CuMn_2O_4 calcined at 600°C for 4 h

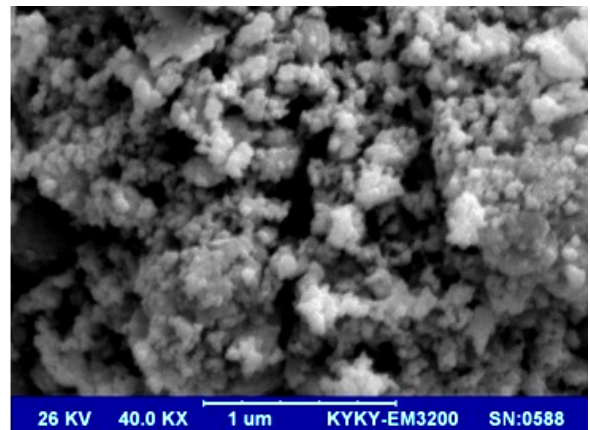


Fig. 4. SEM of the CuMn_2O_4 calcined at 600°C for 4h

cles. The average crystallite size (D) of the sample is found to be 39 nm, calculated using Scherrer formula, which is in agreement with the observation from the SEM results.

The surface morphologies of CuMn_2O_4 nanoparticles are shown in Fig. 4. The Scanning Electron Micrographs (SEM, KYKY-EM3200) of the products revealed that the surface morphology of CuMn_2O_4 particles is quasi-spherical. However, the narrow distribution of the particles with homogeneous size distributions in CuMn_2O_4 reveals approximately a nanoscale particle formation. However, a heterogeneous morphology of CuMn_2O_4 nanoparticles indicates an agglomerated grain structure. In this structure, the average particle sizes are about 39 nm.

Physical Analysis

The optical band gap of CuMn_2O_4 nanoparticles measured using Diffuse Reflectance Spectroscopy (DRS, SCINCO S4100). UV-Vis DRS of synthesized CuM-

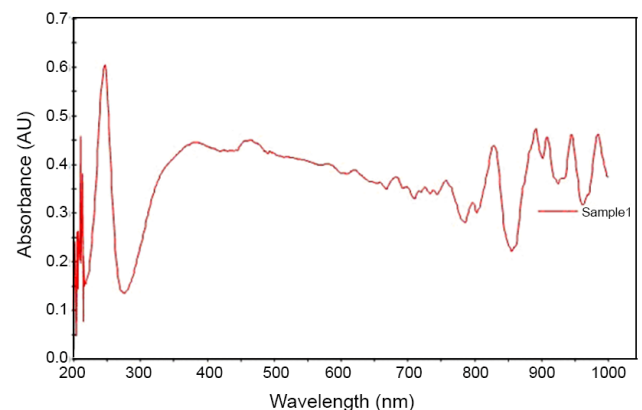


Fig. 5. Absorption versus wavelength behavior of CuMn_2O_4 nanoparticles by DRS

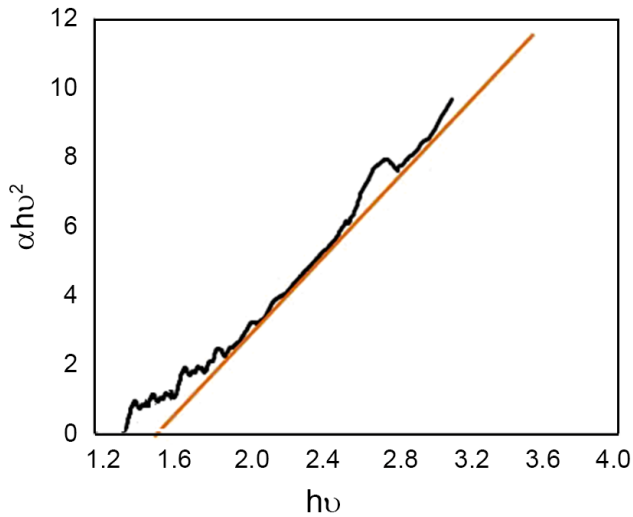


Fig. 5. Absorption versus wavelength behavior of CuMn_2O_4 nanoparticles by DRS

CuMn_2O_4 nanoparticles were obtained between 200 and 1000 nm (Fig. 5). This curve shows a sharp absorbance peak around 250 nm.

The energy gap (E_g) is an important feature of semiconductors, determines their applications in optoelectronics (Khandekar *et al.*, 2014, Masi *et al.*, 2015, Zhang *et al.*, 2012). A common route for extracting band gap from absorption spectra is to get the first derivative of absorbance with respect to photon energy and finding the maximum in the derivative spectra at the lower energy sides (Enhessari *et al.*, 2013). The Tauc model (2) was used to determine the nature of the optical inter-band transition and value of the energy gap E_g .

$$(\alpha h\nu)^2 = A(h\nu - E_g) \quad (2)$$

where α , A , $h\nu$ and E_g are the absorption coefficient, edge width parameters independent of photon energy, energy of incident photon and band gap of the ma-

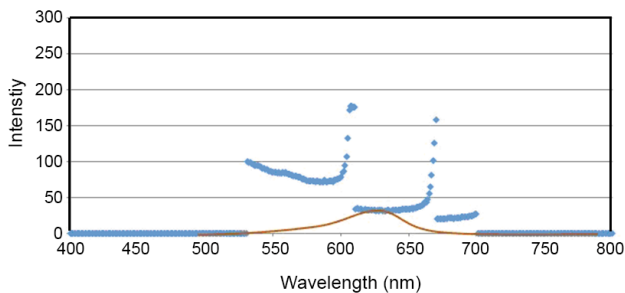


Fig. 7. PL of CuMn_2O_4 nanoparticles

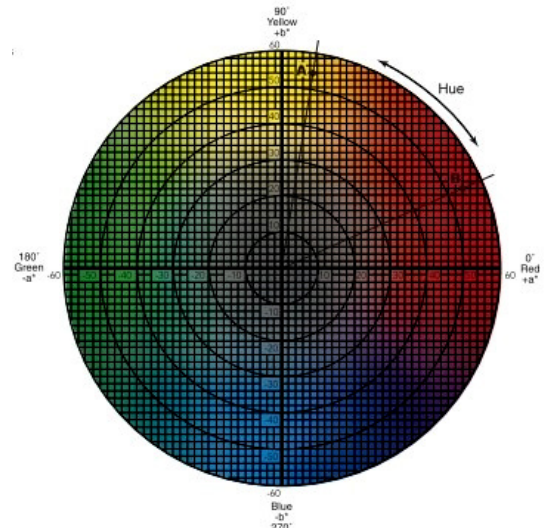


Fig. 8. Arrangement of color attributes in the CIE 1976 ($L^*.a^*.b^*$) color space

terial, respectively. The band gap was obtained by extrapolating the straight portion of the graph on $h\nu$ axis at $(\alpha h\nu)^2$ values (Fig. 6). The results of optical absorption curve has been demonstrated that the band gap of CuMn_2O_4 are about 1.4 eV. Hence, CuMn_2O_4 nanoparticles are semiconductor and can be used in photoelectric devices.

Emission optical spectra have been analyzed at room temperature PL (Perkin Elmer, LS-55 spectrofluorimeter equipped with a xenon discharge lamp) spectrometer. PL spectra of the CuMn_2O_4 nanoparticles (Fig. 7) shows that the main peak of CuMn_2O_4 nanoparticles appears with a general broadening of the PL spectrum around 540-670 nm. The broadening of the spectrum with a weak intensity revealed that the CuMn_2O_4 nanoparticles are subjected to a medium material in photoluminescence applications due to forbidden spin of Mn^{2+} (d^5).

The color scale parameters ($L^*.a^*.b^*$) of CuMn_2O_4 nanoparticles was identified using Reflectance Spectrophotometer (RS, Ihara spcam spectrophotometer). The $L^*.a^*.b^*$, or CIE Lab, color space (Fig. 8) is an international standard for color measurements, adopted by the Commission Internationale d'Eclairage (CIE) in 1976. L^* is the luminance or lightness component, 0-100, and parameters a^* (from green to red) and b^* (from blue to yellow) are the two chromatic components, -60 - +60 (Shaterian *et al.*, 2013). In current study, the L^* , a^* , and b^* parameters obtained at 20.18,

2.98 and 2.94, respectively.

CONCLUSIONS

Spinel CuMn_2O_4 was synthesized successfully via a sol-gel process. The physiochemical characterization of CuMn_2O_4 revealed that a formation of M-O bond at 491 and 606 cm^{-1} , a cubic and nanoscale crystalline phase of CuMn_2O_4 contaminant minor impurities, band gap energy about 1.4eV, and color scale parameters ($L^*.a^*.b^*$) obtained at 20.18, 2.98 and 2.94. Hence, CuMn_2O_4 is a potential semiconducting material with tunable functionalities which can be used as a semiconductor in photoelectric devices.

ACKNOWLEDGEMENT

The authors express gratitude and thanks to Islamic Azad University and Iranian Nanotechnology Initiative Council for supporting this study.

REFERENCES

- Atkins P, Overton T, Rourke J, Weller M and Armstrong F (2006). *Inorganic Chemistry* (Fourth.). USA.
- Byrappa K and Yoshimura M (2001). Hydrothermal Synthesis and Crystal Growth of Fluorides, Sulfides, Tungstates, Molybdates, and Related Compounds. *Handbook of Hydrothermal Technology*, 618–690.
- Enhessari M (2013). Synthesis, characterisation and optical band gap of $\text{Cr}_{1.3}\text{Fe}_{0.7}\text{O}_3$ nanopigments. *Pigment & Resin Technology* 42(4): 347–352.
- Enhessari M, Ozaee K, Shaterian M and Karamali E (2013). Strontium creat nanoparticle synthesis method. US 8512654 B2, 1–6.
- Enhessari M, Shaterian M, Esfahani MJ and Motaharian MN (2013). Synthesis, characterization and optical band gap of La_2CuO_4 nanoparticles. *Materials Science in Semiconductor Processing*. Elsevier 16(6): 1517–1520.
- Ianos R, Roxana B and Borc S (2012). Nanocrystalline BaAl_2O_4 powders prepared by aqueous combustion synthesis. *Ceramics International* 39(2): 2645–2650.
- Ishihara T (2009). *Perovskite Oxide for Solid Oxide Fuel Cells*.
- Kalyani P and Kalaiselvi N (2005). Various aspects of LiNiO_2 chemistry: A review. *Science and Technology of Advanced Materials* 6(1): 689–703.
- Khandekar MS, Tarwal NL, Mulla IS and Suryavanshi SS (2014). Nanocrystalline Ce doped CoFe_2O_4 as an acetone gas sensor. *Ceramics International*. Elsevier 40(1 PART A): 447–452.
- Masi S, Colella S, Listorti A, Roiati V, Liscio A, Palermo V, Rizzo A and Gigli G (2015). Growing perovskite into polymers for easy-processable optoelectronic devices. *Scientific reports* 5(1): 7725.
- Mungse P, Saravanan G, Uchiyama T, Nishibori M, Teraoka Y, Rayalu S and Labhsetwar N (2014). Copper-manganese mixed oxides: CO_2 -selectivity, stable, and cyclic performance for chemical looping combustion of methane. *Physical chemistry chemical physics : PCCP* 16(36): 19634–42.
- Oh K-H, Lee D, Choo M-J, Park KH, Jeon S, Hong SH, Park J-K and Choi JW (2014). Enhanced durability of polymer electrolyte membrane fuel cells by functionalized 2D boron nitride nanoflakes. *ACS applied materials & interfaces*. American Chemical Society 6(10): 7751–8.
- Shaterian M, Barati M, Ozaee K and Enhessari M (2013). Application of MnTiO_3 nanoparticles as coating layer of high performance $\text{TiO}_2/\text{MnTiO}_3$ dye-sensitized solar cell. *Journal of Industrial and Engineering Chemistry* 20(1): 3646–3648.
- Shaterian M, Enhessari M, Rabbani D and Asghari M (2014). Synthesis, characterization and photocatalytic activity of LaMnO_3 nanoparticles. *Applied Surface Science*. 318(2): 213–217.
- Shoemaker DP, Li J and Seshadri R (2009). Unraveling atomic positions in an oxide spinel with two Jahn-Teller ions: local structure investigation of CuMn_2O_4 . *Journal of the American Chemical Society*. American Chemical Society 131(32): 11450–11457.
- Sun S, Wen Z, Jin J, Cui Y and Lu Y (2013). Synthesis of ordered mesoporous CuCo_2O_4 with different textures as anode material for lithium ion battery.

- Microporous and Mesoporous Materials 169 (4): 242–247.
- Uchimoto Y, Amezawa K, Furushita T, Wakihara M and Taniguchi I (2005). Charge-transfer reaction rate at the LiMn_2O_4 spinel oxide cathode/polymer electrolyte interface. *Solid State Ionics* 176(31-34): 2377–2381.
- Zhang Y, Chen Y, Zhang Y, Cheng X, Feng C, Chen L, Zhou J and Ruan S (2012). Chemical A novel humidity sensor based on NaTaO_3 nanocrystalline. *Sensors & Actuators: B. Chemical*. 174 (3): 485–489.

AUTHOR (S) BIOSKETCHES

Morteza Enhessari, Assistant Professor, Department of Chemistry, Naragh Branch, Islamic Azad University, Naragh, Iran, *Email: enhessari@gmail.com*

Ali Salehabadi, PhD., Department of Chemistry, Naragh Branch, Islamic Azad University, Naragh, Iran

Kamal Maarofian, M.Sc., Mahabad Branch, Islamic Azad University, Mahabad, Iran

Salah Khanahmadzadeh, Associate Professor, Department of Chemistry, Mahabad Branch, Islamic Azad University, Mahabad, Iran